

Dynamical Evolution of Protoplanetary Disks

Scott J. Kenyon

Smithsonian Astrophysical Observatory, 60 Garden Street, Cambridge, MA 02138 USA

Abstract. This paper reviews the theory of protostellar debris disks. After a brief introduction to accretion disk physics, I describe coagulation models of planet formation in the outer regions of planetesimal disks. Coagulation models for the Kuiper Belt produce Pluto-sized objects on timescales of 10–40 Myr. These models yield size distributions which agree with observations of Kuiper Belt objects with red magnitudes, $R \approx 20$ –27. Velocity stirring models for other debris disk systems demonstrate that 500 km or larger objects can stir the velocities of small objects up to the shattering limit needed to begin a collisional cascade.

1. Introduction

In the past two decades, several remarkable discoveries have radically altered our understanding of planet formation. In 1983, data from the *Infrared Astronomical Satellite* revealed substantial mid-infrared emission from three A-type main-sequence stars, α Lyr, α PsA, and β Pic (Aumann *et al.* 1983). In addition to the flux expected from an A-type stellar photosphere, the observations implied a cold, extended source of radiation. These data led to a beautiful ground-based image of an edge-on dusty disk surrounding β Pic (Smith & Terrile 1984). This image provided dramatic evidence that the building blocks for solar systems exist in disk-like structures around other stars. More recent images with the *Hubble Space Telescope* and large ground-based telescopes have revealed disks with similar sizes, 100–1000 AU, around many pre-main sequence and main sequence stars (e.g., Jayawardhana *et al.* 1998; Koerner *et al.* 1998; Greaves *et al.* 1998; Augereau *et al.* 1999; Schneider *et al.* 1999; see also the reviews by Beckwith and Koerner in this volume). As in α Lyr and β Pic, all of these systems have excess near-infrared or mid-infrared emission compared to a normal stellar photosphere. More than 50% of young stars (~ 1 Myr) in nearby star-forming regions also have excess infrared emission, suggesting that most stars are born with disks with sizes and masses at least as large as our solar system (e.g., Lada 1999; Jayawardhana *et al.* 1999).

Ground-based radial velocity surveys have recently detected ~ 50 Jupiter-mass and Saturn-mass planets in close orbits around $\sim 1\%$ of nearby solar-type stars (e.g., Latham *et al.* 1989; Marcy & Butler 1996, 1999; Cochran *et al.* 1997; Noyes *et al.* 1997; DelFosse *et al.* 1998). Several systems have multiple planets. Although some of these planet candidates may have masses close to the hydrogen-burning limit for main sequence stars, these discoveries demonstrate

that gas giant planets are relatively common in the solar neighborhood. However, no planet has yet been unambiguously detected in a debris disk system. Rings, warps, and other spatially extended structures in some images suggest the tidal influence of planets embedded in several debris disks (e.g., Kalas & Jewitt 1995), but direct detection of planetary motion has proved difficult.

The final interesting discovery links extra-solar disks and planets with the formation and evolution of our solar system. Recent surveys have detected a substantial population of Kuiper Belt objects (KBOs), small icy bodies outside the orbit of Neptune (Luu & Jewitt 1988, 1998; Luu *et al.* 1997; Jewitt & Luu 1993). For an adopted albedo of 4%, known KBOs have radii of 50–500 km. The measured surface density of KBOs on the sky suggests a total mass of $\sim 0.1\text{--}0.3 M_{\oplus}$ (Luu & Jewitt 1998; Jewitt *et al.* 1998; Trujillo *et al.* 2000; Kenyon & Windhorst 2000). With semimajor axes of 40–50 AU and orbital inclinations of $0^{\circ}\text{--}30^{\circ}$, the apparent geometry and mass of the KBO population is similar to results derived for the dusty disks observed in α Lyr and β Pic, suggesting that phenomena currently observed in extra-solar dusty disks probably occurred early in the formation of our own solar system.

These discoveries have fueled interest in theoretical studies of planet formation in a variety of astrophysical contexts. This paper reviews some of these studies, with an emphasis on the dynamical evolution of planetary debris disks (for other reviews, see chapters in Mannings, Boss, & Russell 2000). After starting with a short summary of current models for planet formation, I consider in detail several recent numerical calculations of planet formation in debris disks and describe observational tests of these models. I conclude with a discussion of future prospects for the calculations and with suggestions for observations to test different models of planet formation.

2. Basic Theory

2.1. Background

Standard models for planet formation begin with a circumstellar disk surrounding a newly-formed star (Beckwith 1999; Lada 1999). The disk consists of numerous small dust grains embedded in a more massive, gaseous nebula which rotates about the central star. The disk mass is $\lesssim 10\%\text{--}20\%$ of the mass of the central star. The internal energy of the gas in the disk is also small compared to the energy of the gravitational potential; the gas thus has a small local scale height compared to the distance from the central star. The small velocity shear between adjacent disk annuli heats the disk; energy lost to viscous heating causes mass to move inwards and angular momentum outwards.

Two basic theories – coagulation and dynamical instability – predict that planets can form and survive in this environment. In the coagulation theory, large dust grains within the disk decouple from the gas and settle to the mid-plane. These grains may then coagulate into successively larger grains (e.g., Weidenschilling 1980; Weidenschilling & Cuzzi 1993) or continue to settle into a very thin layer which can become gravitationally unstable (e.g., Goldreich & Ward 1973). Both paths produce km-sized planetesimals which collide and merge to produce larger bodies. If the growth time is short compared to the viscous timescale, collisions and mergers eventually produce one or more ‘cores’

which accumulate most, if not all, of the solid mass in an annular ‘feeding zone’ defined by balancing the gravity of the growing planetesimal with the gravity of the Sun and the rest of the disk. Large cores with masses of $1\text{--}10 M_{\oplus}$ can also accrete gas from the feeding zone (Pollack 1984). Applied to our solar system, this model can account for the masses of the terrestrial and several gas giant planets (e.g., Lissauer *et al.* 1996; Pollack *et al.* 1996; Weidenschilling *et al.* 1997; Levison *et al.* 1998; but see Boss 1997, 2000). Variations of this model, including orbital migration and other dynamical processes, are invoked to explain Jupiter-sized planets orbiting other solar-type stars (e.g., Weidenschilling & Marzari 1996, Lin & Ida 1997; Ford *et al.* 1999; Kley 2000).

Dynamical instability models focus on the possibility that part of an evolving disk can collapse directly into a Jupiter-mass planet (Boss 1997, 2000; see also Cameron 1995 and references therein). If the local surface density is large enough to overcome local shear and pressure forces, part of the disk begins to collapse. Cool material flows into the growing perturbation, which aids the collapse. Eventually, the perturbation achieves planet-sized proportions by accumulating all of the gaseous and solid material in the feeding zone. This model has a natural advantage over coagulation models: the collapse is rapid, $\sim 10^3$ to 10^5 yr, compared to the 1–10 Myr lifetime of gaseous disks surrounding nearby pre-main sequence stars (Russell *et al.* 1996; Hartmann *et al.* 1998; Lada 1999). Coagulation models barely succeed in making gas giant planets in 1–10 Myr. However, the disk mass needed to start a dynamical instability may exceed the mass typically observed in pre-main sequence disks (Beckwith 1999; Lada 1999). Dynamical instability models produce neither terrestrial planets in the inner disk nor icy bodies like Pluto in the outer disk.

2.2. Disk Physics

Calculations for both planet formation models require a good understanding of the important physical processes in the disk. Gas and solid particles in the disk interact with each other and with the gravitational potential and the radiation field of the central star. For the purposes of this review, I ignore interactions with external objects, such as nearby stars, molecular clouds, and the tidal field of the galaxy. During the late stages of planet formation, these interactions are important for shaping the evolution of the outermost portions of a solar system, at distances of $\sim 10^3$ to 10^4 AU from the central star (see Duncan, Quinn, & Tremaine 1987, Teplitz *et al.* 1999, and references therein). External forces can also deliver stochastic dynamical perturbations to the inner disk, which may aid or inhibit planet formation depending on the magnitude of the perturbation (see, for example, Ida *et al.* 2000; Kalas *et al.* 2000).

The basic driving mechanism of an isolated gaseous disk is the viscosity, which acts to transport mass radially inwards and angular momentum radially outwards (von Weiszäcker 1943, 1948; see Lin & Papaloizou 1995, 1996 and Hartmann 1998 for recent reviews). To understand how this process works, consider a thin ring with two adjacent annuli at distances r_1 and r_2 from a central star (Figure 1). Material in these annuli orbits the central star with velocities, v_1 and v_2 . The velocity difference between the two annuli, $v_1 - v_2 > 0$, produces a frictional force that attempts to equalize the two orbital velocities. The energy lost to friction heats the annuli; some disk material then

moves inwards to conserve total energy. This inward mass motion increases the angular momentum of the ring; some disk material moves outwards to conserve angular momentum. Energy and angular momentum conservation thus lead to an expansion of the ring in response to frictional heating. The ring eventually expands into a disk, which generates heat (and radiation) at a level set by the rate mass moves through the disk, \dot{M} , known as the accretion rate.

In addition to viscous heating, several other processes change the structure of an accretion disk. Disks can lose mass and angular momentum in a wind, which can be driven by direct radiative acceleration or from magnetic energy (e.g., Shu *et al.* 1994a,b; Najita & Shu 1994; Ostriker & Shu 1995; Proga *et al.* 1998; Proga 2000). High energy photons and mass loss from the central star can heat the disk, raising its energy output (Kenyon & Hartmann 1987; Chiang & Goldreich 1997, 1999), and perhaps increasing the rate of mass loss from the wind or from evaporation (Hartmann & Raymond 1984; Johnstone *et al.* 1998; Richling & Yorke 1997, 1998, 2000). Gaseous disks are also prone to several types of thermal instabilities, which can produce factor of 10–100 changes in the energy output of the disk on timescales ranging from minutes to centuries (Hartmann & Kenyon 1985, 1996; Bell & Lin 1994; Bell *et al.* 1995; Lin & Papaloizou 1995, 1996; Kenyon 1999).



Figure 1 - Schematic view of two adjacent annuli in a disk surrounding a compact star. Annulus '1' lies inside annulus '2' and orbits the star (filled circle) at a higher velocity, $v_1 > v_2$.

The importance of other physical processes in a gaseous disk relative to the viscous heating depends on the source of the viscosity, which remains controversial. Ordinary molecular viscosity is too small to generate mass motion on a reasonable time scale, \sim days for disks in interacting binary systems and \sim years to decades for disks in pre-main sequence stars. The large shear between adjacent disk annuli suggests that disks might be unstable to turbulent motions, which has led to many turbulent viscosity mechanisms. Convective eddies, gravitational instabilities, internal shocks, magnetic stresses, sound waves, spiral density waves, and tidal forces have all been popular turbulence mechanisms in the past three decades (see Kenyon 1999 and references therein).

Recent work has shown that magnetic stresses in a differentially rotating disk inevitably lead to turbulence (Balbus *et al.* 1996; Balbus & Hawley 1998; Stone *et al.* 2000). The growth time and effectiveness of these magnetohydrodynamic mechanisms make them the current leading candidate for viscosity in most applications. How this turbulence leads to significant mass motion in a real accretion disk remains an unsolved problem.

Shakura & Sunyaev (1973) avoided some of the basic physical uncertainties of viscosity mechanisms with the popular “ α -disk” model (see also von Weiszäcker 1943, 1948; Lüst 1952; Lynden-Bell & Pringle 1974). They considered viscosity as a turbulent process, $\nu = \alpha c_s h$, where c_s is the sound speed, h is the local scale height of the gas, and α is a dimensionless constant. This concept is similar to the mixing length theory of convection, with α serving the role of the mixing length. In most applications, $\alpha \lesssim 1-10$; α must exceed $\sim 10^{-4}$ to allow material to move inwards on a reasonable time scale.

2.3. Timescales

This viscosity definition orders the important time scales for gas in the disk (Lynden-Bell & Pringle 1974). The shortest disk time scale is the dynamical (orbital) time scale, which increases radially outward:

$$\tau_D \approx 1000 \text{ yr} \left(\frac{A}{100 \text{ AU}} \right)^{3/2} \left(\frac{1 \text{ M}_\odot}{M_*} \right)^{-1/2} \quad (1)$$

The thermal time scale measures the rate that energy diffuses through the disk,

$$\tau_T \approx 5000 \text{ yr} \left(\frac{A}{100 \text{ AU}} \right)^{11/8} \quad (2)$$

The thermal time scale is intermediate between the dynamical time scale and the viscous time scale, which measures the rate matter diffuses through the disk,

$$\tau_V \approx \frac{25,000 \text{ yr}}{\alpha} \left(\frac{A}{100 \text{ AU}} \right)^{5/4} \quad (3)$$

These last two expressions do not include a weak dependence on the mass of the central star. The unknown α parameter sets the viscous timescale; τ_V is more than 10,000 yr at 100 AU for any reasonable α . Most studies of disk evolution suggest $\alpha \sim 10^{-3}$ to 10^{-2} , which yields viscous timescales of 1–10 Myr at 100 AU. Figure 5 of Kenyon (1999) shows how the disk reacts to a perturbation in its structure on each of these timescales.

The final evolutionary timescale for gas in a disk depends on an external source, the central star, instead of internal physics. Hollenbach *et al.* (1994, 2000; also Shu *et al.* 1993; Richling & Yorke 1997, 1998, 2000) showed that high energy photons from a luminous central star can ionize the outer skin of the gaseous disk and raise the gas temperature to $\sim 10^4$ K. The thermal velocity of this gas is large enough to overcome the local gravity for material beyond ~ 10 AU for a 1 M_\odot central star. Material then leaves the disk, producing a bipolar outflow which may be observed in nearby star-forming regions (e.g., Johnstone *et al.* 1998; Bally *et al.* 1998). Disk evaporation occurs on a timescale

$$\tau_E \approx 10^7 \text{ yr} \left(\frac{M_d}{0.01 M_\odot} \right) \left(\frac{A}{10 \text{ AU}} \right) \left(\frac{\phi_\star}{10^{41} \text{ s}^{-1}} \right)^{-1/2}, \quad (4)$$

where ϕ_\star is the flux of hydrogen-ionizing photons from the central star.

The physics of dust evolution in the disk is equally complicated. Low velocity collisions between dust particles probably produce larger dust particles; high velocity collisions produce debris. Radiation pressure can eject small dust grains; gas drag and Poynting-Robertson drag can pull small grains into the central star if stellar radiation does not evaporate them first. Although small dust grains initially orbit the central star in roughly circular orbits, drag forces and long-range gravitational perturbations can modify their orbits significantly over time. Angular momentum transfer during elastic collisions – viscous stirring – increases the eccentricity and inclination of all solid bodies in the disk. Kinetic energy transfer during elastic collisions – dynamical friction – leads to “energy equipartition,” where the most massive objects have more nearly circular orbits than less massive objects (see Ida & Makino 1992, 1993).

Despite these complications, we can order the timescales for dust evolution in the disk. Ejection of dust grains by radiation pressure occurs on the local dynamical timescale, equation (1), the shortest timescale in the disk. The coagulation timescale is very sensitive to the particle size and the local particle density, and can range from days to months for small grains in a dense medium (see Cuzzi *et al.* 1993; Wurm & Blum 1998, 2000) to many Gyr for large planets in a very low density medium. The timescale for grains to settle to the mid-plane, and the possible onset of a gravitational instability within this material, depends on the magnitude and source of turbulence in the disk, of which little is known. In current theories, the timescale to produce cm-sized to km-sized objects is long compared to the local dynamical time but short compared to the thermal timescale of the gaseous disk (e.g., Goldreich & Ward 1973; Weidenschilling 1980; Weidenschilling & Cuzzi 1993; Sekiya & Ishitsu 2000). Larger objects are inevitable as long as the collision velocity in the disk remains low. The timescale to make 1000 km objects in a particle disk is:

$$\tau_G \approx 10^8 \text{ yr} \left(\frac{A}{100 \text{ AU}} \right)^{2.5} \left(\frac{M_d}{0.01 M_\odot} \right)^{-1}, \quad (5)$$

The growth time is more sensitive to the location in the disk than the mass of the disk. Once 1000 km objects form, larger objects can often grow quickly; thus τ_G is a useful reference for most large planets.

Two processes prevent coagulation from producing extremely massive objects, drag forces and long-range gravitational perturbations. Gas drag and Poynting-Robertson drag remove small objects from the nebula on timescales,

$$\tau_{GD} \approx 10^6 \text{ yr} \left(\frac{m_i}{10^9 \text{ g}} \right)^{1/3} \left(\frac{A}{100 \text{ AU}} \right)^{1/2} \left(\frac{1 \text{ M}_\odot}{M_\star} \right)^{1/2} \left(\frac{10^{-14} \text{ g cm}^{-3}}{\rho_g} \right) \quad (6)$$

for gas drag (Adachi *et al.* 1976; Kary *et al.* 1993; 10 m objects have $m_i \sim 10^9$ g) and

$$\tau_{PR} \approx 10^7 \text{ yr} \left(\frac{R}{1 \text{ } \mu\text{m}} \right) \left(\frac{A}{100 \text{ AU}} \right)^2 \left(\frac{L_\star}{1 \text{ L}_\odot} \right)^{-1}, \quad (7)$$

for Poynting-Robertson drag (Burns *et al.* 1979). Gas drag is effective on objects smaller than ~ 1 km when the gas density in the nebula is large. Poynting-Robertson drag is important when high velocity collisions produce large amounts of debris in nebulae with little gas content. The gravitational perturbations viscous stirring and dynamical friction are important throughout the evolution of a dusty nebula. The timescale for viscous stirring is comparable to the growth time; dynamical friction usually acts on a shorter timescale.

Once the largest objects reach their ‘maximum’ size, they rapidly stir up the velocities of the smallest objects. When the velocities are large enough, collisions tend to produce debris instead of mergers. Once collisions produce large amounts of debris, the debris will continue to shatter. The timescale to remove bodies from the nebula in this “collisional cascade” is (Kenyon & Bromley 2001; see also Backman *et al.* 1995; Artynowicz 1997; Lagrange *et al.* 2000)

$$\tau_C \approx 5 \times 10^8 \text{ yr} \left(\frac{A}{100 \text{ AU}} \right)^3 \left(\frac{M_d}{0.01 \text{ M}_\odot} \right)^{-1}. \quad (8)$$

With these timescales in place, we can develop a simple understanding of planet formation in a gaseous disk with some solid material at the disk midplane (see Figure 2). This picture depends on observations of typical sizes, ~ 100 – 1000 AU, and masses, $\sim 10^{-3}$ to 10^{-1} M_\odot , for circumstellar disks surrounding nearby stars (see Lagrange *et al.* 2000; Beckwith, this volume; Koerner, this volume). For reasonable choices of the viscosity coefficient, $\alpha \sim 10^{-3}$ to 10^{-2} , and the ionization rate of the central star, $\phi_\star \sim 10^{41} \text{ s}^{-1}$, the timescale for the disappearance of gas in the disk is 1–10 Myr (see equations (3) and (4)). This timescale is similar to the observed upper limit to the lifetime of gaseous disks in the solar neighborhood and nearby star-forming regions, $\lesssim 10$ – 100 Myr.

As the gas evolves, dust grains coagulate and grow to mm or cm sizes on short timescales in the dusty midplane. If the dust layer becomes gravitationally unstable, these objects can grow to km-sized objects relatively quickly. Otherwise, continuing coagulation gradually produces objects with radii of 1 m to 1 km. In either case, coagulation continues to produce larger and larger objects. These objects begin to accrete gas on timescales which are very sensitive to the distance from the central star, equation (5). For $M_d \gtrsim 0.01 \text{ M}_\odot$ and $A \lesssim 10$ – 20 AU, coagulation models can produce gas giant planets before the gas disappears. Coagulation models currently fail to produce gas giant planets at larger distances from the central star for any reasonable disk mass on timescales of 10 Myr or smaller (see Nakagawa *et al.* 1983; Fernández & Ip 1984; Lissauer 1987, 1993, 1995; Ip 1989; Pollack *et al.* 1996).

Once the gas has dispersed, coagulation can continue to produce large solid objects at ~ 1 AU and at $\gtrsim 20$ – 30 AU from the central star. Gravitational perturbations from the gas giants and the largest solid bodies stir up the velocities of the smaller objects left over from the accumulation process. Collisions between these small bodies produces debris which is ejected by radiation pressure, dragged inwards by Poynting-Robertson drag, or incorporated into larger bodies. This process continues for the age of the solar system, although the

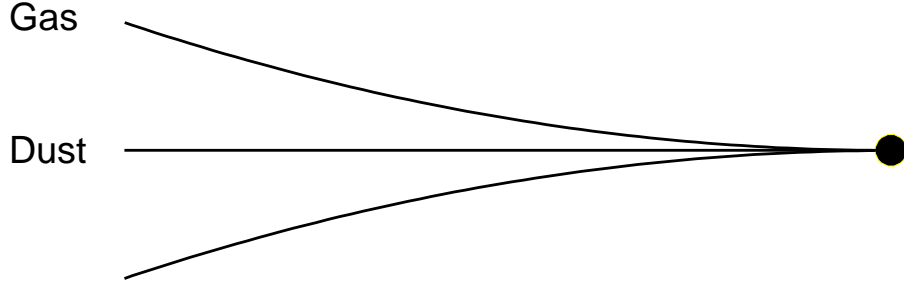


Figure 2 - Schematic side view of a protostellar disk. Large dust grains settle to the midplane and have a dynamical scale height, H_d , defined by the velocity dispersion about a circular orbit. In most cases, $H_d/A \sim 10^{-2}$ to 10^{-3} . The gas is in vertical hydrostatic equilibrium and has a scale height H_g above the midplane; H_g is set by the local gas temperature derived from viscous heating and the absorption of stellar photons. Gaseous disks usually have $H_d/A \sim 0.1$ –1.0 at $A \sim 100$ AU (Kenyon & Hartmann 1987).

debris of extra-solar disks probably can be observed for only ~ 1 Gyr (equation 8; Habing *et al.* 1999; Lagrange *et al.* 2000).

To add quantitative details to this picture, we must calculate the evolution of the gas and dust in a circumstellar disk using a numerical model for each physical process. Various groups have developed sophisticated numerical codes to follow the evolution of (i) the gas (e.g., Ruden & Pollack 1991; Pollack *et al.* 1996; Bodenheimer *et al.* 2000; Boss 2000; Kley 2000), (ii) the dust (e.g., Greenberg *et al.* 1978, 1984; Wetherill & Stewart 1989, 1993; Spaute *et al.* 1991; Weidenschilling *et al.* 1997; Kenyon & Luu 1998, 1999; Kortenkamp & Wetherill 2000), and (iii) the gas and dust (e.g., Bryden *et al.* 2000; Klahr & Lin 2001). To illustrate the results of these calculations, I will now describe coagulation calculations for the outer part of our solar system (Kenyon & Luu 1998, 1999) and the velocity evolution of small particles in a debris disk (Kenyon & Bromley 2001).

3. Coagulation Calculations

To calculate the growth of planets from small dust grains, Safronov (1969) developed the particle-in-a-box method, which treats planetesimals as a statistical ensemble of masses with a distribution of horizontal, h_i , and vertical, v_i , velocities about a circular orbit. Wetherill & Stewart (1989, 1993), Spaute *et al.* (1991), Weidenschilling *et al.* (1997), and Kenyon & Luu (1998) include references to early work on this subject. A statistical approach is essential, because it is not possible to follow the evolution of 10^{15} or more small planetesimals with modern n -body codes. Our calculations begin with a differential mass distribution, $n(m_i)$, in concentric annuli centered at heliocentric distances, A_j , from a star of mass M_\star (Kenyon & Luu 1998, 1999; Kenyon & Bromley 2001). We divide this distribution among N mass batches, where $\delta_i \equiv m_{i+1}/m_i$ is the mass spacing between each batch. Most calculations have $\delta = 1.1$ –2.0. To evolve the mass and velocity distributions in time, we solve the coagulation and energy con-

servation equations for an ensemble of objects with masses ranging from $\sim 10^7$ g to $\sim 10^{26}$ g. We adopt analytic cross-sections to derive collision rates, use the center-of-mass collision energy to infer the collision outcome (merger, merger + debris, rebound, or disruption), and compute velocity changes from gas drag and collective interactions such as dynamical friction and viscous stirring using a Fokker-Planck integrator (Stewart & Ida 2000; see also Hornung *et al.* 1985; Barge & Pellat 1990; Luciani *et al.* 1995). Our code has passed numerous tests, such as matching the results of analytic solutions to the coagulation equation (Wetherill 1990; see also Lee 2000; Malyshkin & Goodman 2000) and complete calculations at 1 AU (e.g., Wetherill & Stewart 1993).

3.1. The Minimum Mass Solar Nebula

Before describing several coagulation calculations, it is useful to introduce the ‘Minimum Mass Solar Nebula,’ the minimum amount of material needed to build the planets of our solar system (see Weidenschilling 1977, Hayashi 1981, Bailey 1994, and references therein). Hoyle (1946) first emphasized the importance of this concept as a starting point for theories of solar system formation. The Minimum Mass is based on the close parallel between the measured elemental compositions of the earth, Moon, and meteorites and the relative abundances of heavy elements in the Sun (see the discussion in Harris 1978). This result leads to the assumption that the initial abundance of the solar nebula is similar to the solar abundance. The Minimum Mass Solar Nebula follows from adding hydrogen and helium to each planet to reach a solar abundance and spreading the resulting mass uniformly over an annulus centered on the orbit of the planet.

Figure 3 shows how the mass surface density varies with distance for the Minimum Mass Solar Nebula. The arrows indicate the mass added to the terrestrial planets. The plot shows Venus, the Earth, Jupiter, Saturn, Uranus, Neptune, and the Kuiper belt. When the material at the orbits of Venus and the Earth is augmented to reach a solar abundance of hydrogen, the surface density for the gas follows the solid curve, $\Sigma_g \approx \Sigma_0 (A/1 \text{ AU})^{-3/2}$, out to $A \approx 10$ AU and then decreases sharply. The solid curve in Figure 1 has $\Sigma_0 = 1500 \text{ g cm}^{-2}$; for comparison, Hayashi *et al.* (1985) proposed $\Sigma_0 = 1700 \text{ g cm}^{-2}$ while Weidenschilling (1977) suggested $\Sigma_0 = 3200 \text{ g cm}^{-2}$. Following Hayashi (1981), the dot-dashed curve has

$$\Sigma_s = \begin{cases} 7 \text{ g cm}^{-2} (A/1 \text{ AU})^{-3/2} & A \leq 2.7 \text{ AU} \\ 30 \text{ g cm}^{-2} (A/1 \text{ AU})^{-3/2} & A > 2.7 \text{ AU} \end{cases} \quad (9)$$

The uncertainties in the coefficients are again a factor of ~ 2 . The change in the surface density of solid material at 2.7 AU corresponds to the region where ice condenses out of the gas in Hayashi’s (1981) model. The location of this region depends on the disk structure (Sasselov & Lecar 2000).

The Minimum Mass Solar Nebula was one of the great successes of early viscous accretion disk theories, because steady-state disk models often yield $\Sigma \propto A^{-3/2}$. The sharp decrease in Σ at 10–30 AU supports photoevaporation models, because ionized hydrogen becomes unbound at ~ 10 AU (Shu *et al.*

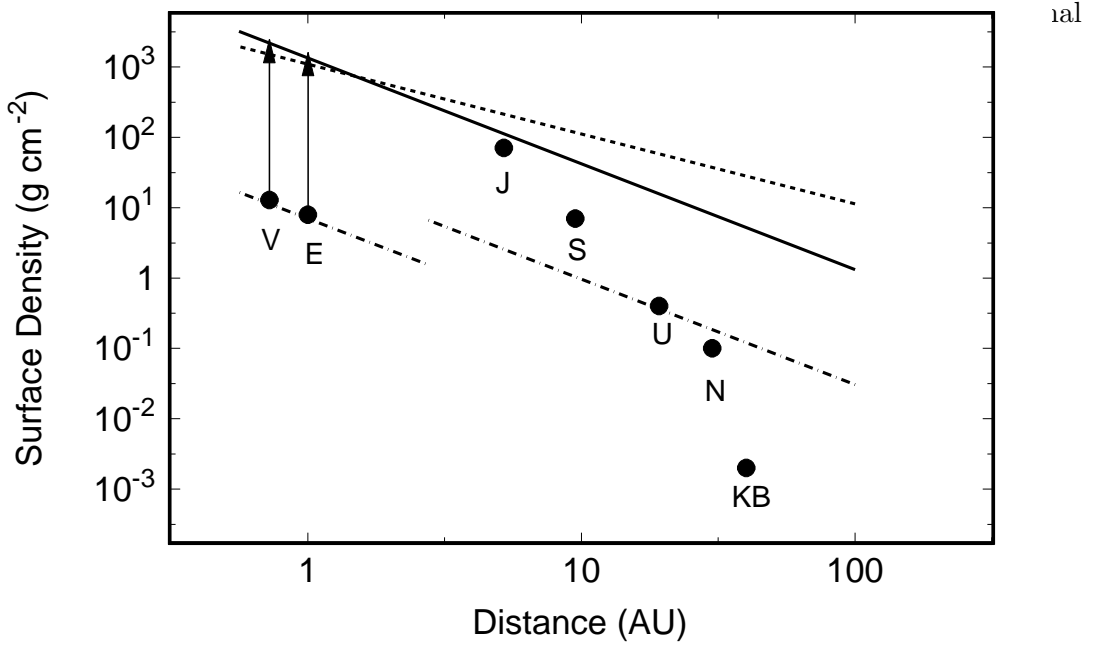


Figure 3 - Surface density distribution in the solar system, assuming that the mass is spread uniformly over an annulus centered on the orbit of the planet. The arrows indicate the surface density for terrestrial planets if augmented to a solar hydrogen abundance. The solid and dot-dashed curves indicate $\Sigma \propto A^{-3/2}$; the dashed line indicates $\Sigma \propto A^{-1}$ (Cameron 1995).

1993). Current abundance measurements for the gas giants lend additional evidence: the gas-to-dust ratio appears to decrease with radius in parallel with the surface density drop beyond 10 AU (Pollack 1984; Podolak *et al.* 1985; Podolak & Reynolds 1987; Pollack *et al.* 1996). In the Kuiper Belt, there may be two origins for the additional large drop in surface density from a $\Sigma \propto A^{-3/2}$ model. Adding H and He at 30–40 AU increases the mass in the Kuiper Belt by a factor of ~ 30 . Material lost to high velocity collision of objects in the Belt increases the mass by another factor of 10–100 (e.g., Holman & Wisdom 1993; Davis & Farinella 1997; Kenyon & Luu 1999a, b), bringing the initial surface density in the Kuiper Belt within range of the $\Sigma \propto A^{-3/2}$ line. If these estimates are correct, the total mass of the Minimum Mass Solar Nebula is $\sim 0.01 M_\odot$ for an outer radius of ~ 100 AU, close to the median mass for circumstellar disks surrounding young stars in nearby regions of star formation (Lada 1999).

Figure 4 suggests that the Kuiper Belt provides an important test of coagulation models. Forming objects with radii of ~ 500 –1000 km requires $\sim 10^7$ yr at ~ 40 AU in a Minimum Mass Solar Nebula (equation (5)). The outermost gas giant, Neptune, must form on a similar timescale to accrete gas from the solar nebula before the gas escapes (equation (3)). Neptune formation places another constraint on the KBO growth time, because Neptune inhibits KBO formation at 30–40 AU by increasing particle random velocities on timescales of 20–100 Myr (Holman & Wisdom 1993; Duncan *et al.* 1995; Morbidelli & Valsecchi 1997). Kenyon & Luu (1998, 1999a,b) investigated how KBOs form

by coagulation and compared their results with observations (see also Fernández 1997; Stern & Colwell 1997a, b and references therein). The next section briefly describes the model results; §4 compares these results with observations.

3.2. Kuiper Belt Models

Figure 4 shows the results of a complete coagulation calculation for the Kuiper Belt in our solar system. The input cumulative size distribution N_C is $N_C \propto r_i^{q_0}$, with initial radii $r_i = 1\text{--}80$ m and $q_0 = 3$. We assume these particles are uniformly distributed in a single annulus with a width of 6 AU at 32–38 AU from the Sun. The total mass in the annulus is M_0 ; $M_0 \approx 10 M_{\oplus}$ for a Minimum Mass Solar Nebula. All mass batches start with the same initial velocity. We tested a range of initial velocities corresponding to initial eccentricities of $e_0 = 10^{-4}$ to 10^{-2} , as is expected for planetesimals in the early solar nebula (Malhotra 1995). The adopted mass density, $\rho_0 = 1.5 \text{ g cm}^{-3}$, is appropriate for icy bodies with a small rocky component. Kenyon & Luu (1999a,b) describe these parameters in more detail.

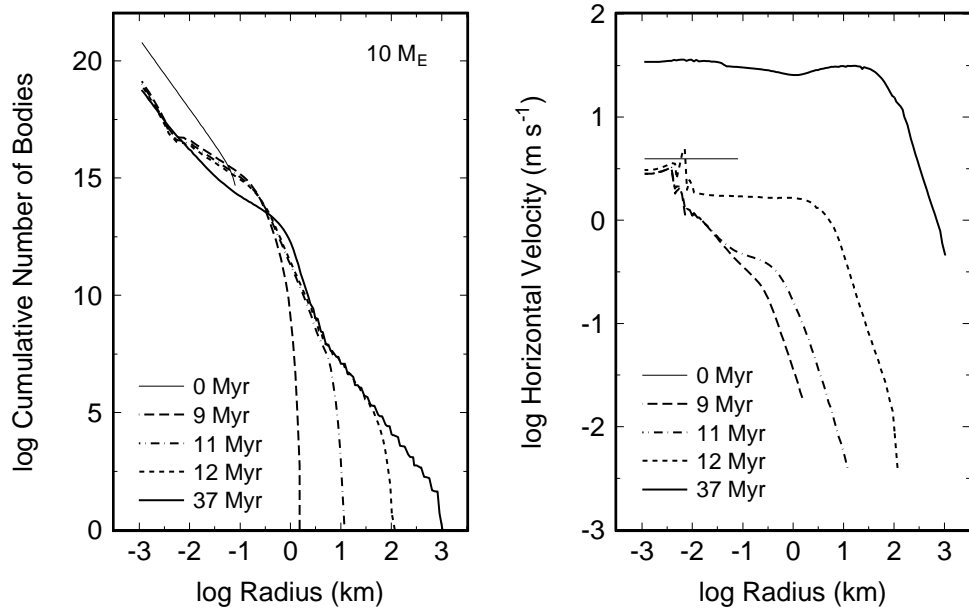


Figure 4 - Cumulative size distributions as a function of time for a model with $M_0 = 10 M_{\oplus}$ from Kenyon & Luu (1999a). The evolution time for each curve is listed in the legend. Crosses indicate observational and theoretical constraints on the size distribution at radii of 50 km, 10 km, and 1 km as described in the text.

We separate the growth of KBOs into three regimes. Early in the evolution, frequent collisions damp the velocity dispersions of small bodies. These bodies slowly grow into 1 km objects on a timescale of 5–10 Myr $(M_0/10 M_{\oplus})^{-1}$. This linear growth phase ends when the gravitational range of the largest objects exceeds their geometric cross-section. This “gravitational focusing” enhances the collision rate by factors of 10–1000. The largest objects then begin a period

of “runaway growth”, when their radii grow from ~ 1 km to $\gtrsim 100$ km in several Myr. During this phase, dynamical friction and viscous stirring increase the velocity dispersions of the smallest bodies from ~ 1 m s $^{-1}$ up to ~ 40 m s $^{-1}$. This velocity evolution reduces gravitational focusing factors and ends runaway growth. The largest objects then grow slowly to 1000+ km sizes on timescales that again depend on the initial mass in the annulus. Kokubo & Ida (1998) call this last phase in the evolution ‘oligarchic growth’ to distinguish it from the linear and runaway growth phases (see also Ida & Makino 1993).

The shapes of the curves in Figure 4 show features common to all coagulation calculations. Almost all codes produce two power-law size distributions, $N_C \propto r_i^{-q_f}$. The merger component at large sizes has $q_f \approx 3$; the debris component at small sizes has $q_f = 2.5$ (Dohnanyi 1969). Dynamical friction produces a power law velocity in the merger component. Because the debris component contains a small fraction of the initial mass, it has roughly constant velocity. The transition region between the two components usually has a ‘bump’ in the size distribution, where objects which can merge grow rapidly to join the merger population. Calculations for annuli closer to the Sun also yield a ‘runaway’ population, a plateau in the size distribution of the largest objects.

Our Kuiper Belt calculations yield one result which is very different from coagulation calculations for annuli at less than 10 AU from the Sun. In all other published calculations, the largest bodies contain most of the initial mass in the annulus. In the Kuiper Belt, most of the initial mass ends up in 1 km objects. Fragmentation and gravitational stirring are responsible for this difference between calculations at 1–10 AU and at 40 AU. In our calculations, fragmentation produces a large reservoir of small bodies that damp the velocity dispersions of the large objects through dynamical friction. These processes allow a short runaway growth phase where 1 km objects grow into 100 km objects. Continued fragmentation and velocity evolution damp runaway growth by increasing the velocity dispersions of small objects. Our models thus enter the phase of ‘oligarchic growth’ earlier than models for planet growth at 1–10 AU. This evolution leaves $\sim 1\%-2\%$ of the initial mass in 100–1000 km objects.¹ The remaining mass is in 0.1–10 km radius objects. Continued fragmentation will gradually erode these smaller objects into dust grains that are removed from the Kuiper Belt on short timescales, $\sim 10^7$ yr (see Backman & Paresce 1993; Backman *et al.* 1995). Thus, in our interpretation, 100–1000 km radius objects comprise a small fraction of the original Kuiper Belt. This conclusion supports the notion that the solar nebula followed the $\Sigma \propto A^{-3/2}$ law out to ~ 40 –50 AU.

The coagulation calculations for the Kuiper Belt also support a link between the formation of large icy objects like KBOs and the evolution of dusty debris disks in α Lyr, β Pic, and other main sequence stars. In our models, the growth of 100–1000 km radius KBOs in the outer solar system is accompanied by substantial dust production, ~ 0.1 –1 M_E , in models with initial surface densities of 1–5 times the Minimum Mass Solar Nebula. This dust mass is comparable to the ‘maximum’ masses inferred for α Lyr and β Pic (e.g., Backman & Paresce 1993; Lagrange *et al.* 2000). The opening angle of the disk in β Pic implies

¹Calculations by Stern (1995, 1996) and Stern & Colwell (1997a,b) do not include a self-consistent algorithm for velocity evolution and thus do not achieve these results.

vertical velocity dispersions of $\sim 100 \text{ m s}^{-1}$, close to that derived for the Kuiper Belt calculations. To explore this connection in more detail, we have begun a set of coagulation calculations appropriate for debris disks surrounding nearby A-type stars. The following section describes our progress.

3.3. Debris Disk Models

Current models for a debris disk envision a collection of dust grains in circular orbits around an A-type star (see Artymowicz 1997; Lagrange *et al.* 2000). For particle sizes of 1–100 μm , Poynting-Robertson drag and radiation pressure remove dust from the disk in ~ 1 –10 Myr (equation (7)). Collisions between larger bodies can replenish small grains if the collision velocity is ~ 100 –300 m s^{-1} . These large velocities initiate a “collisional cascade,” where planetesimals with radii of 1–10 km are ground down into smaller and smaller bodies (Artymowicz *et al.* 1989; Backman *et al.* 1995). A collisional cascade requires a mass reservoir of ~ 10 –100 M_\oplus to replenish smaller grains over a disk lifetime of 100 Myr or more (Artymowicz 1997; Habing *et al.* 1999; Lagrange *et al.* 2000; Kenyon & Bromley 2001).

The origin of the large collision velocities in this picture is uncertain. Because the difference between the gas velocity and dust velocity is small and circularization is efficient, dust grains and larger bodies within a protosolar nebula probably had nearly circular orbits initially. Short-term encounters with passing stars and stirring by planets embedded in the disk can increase the velocities of dust grains (Artymowicz *et al.* 1989; Larwood 1997; Mouillet *et al.* 1997; Ida *et al.* 2000; Kalas *et al.* 2000). Although stellar encounters can increase particle velocities enormously, such encounters are probably rare. Collisions of bodies within the disk may also effectively damp large velocities following the encounter; Kenyon & Luu (1999a) estimate damping times of 1–10 Myr for 1–100 m objects during the early stages of planetesimal growth in the Kuiper Belt. Stirring by embedded planets is attractive, because objects with radii of 1000 km or more naturally form in the outer disk (§3.2) and these objects continuously stir up the velocities of small dust grains (see also Kenyon *et al.* 1999).

Kenyon & Bromley (2001) recently examined the possibility that large objects embedded in a debris disk can stir up the velocities of smaller objects to the ‘shattering limit’ and thus produce a collisional cascade (see also Backman & Paresce 1993; Backman *et al.* 1995; Artymowicz 1997; Kenyon *et al.* 1999; Lagrange *et al.* 2000). Using reasonable physical constants for the grain population, they show that 1 km objects with collision velocities of 100 m s^{-1} or more can replenish the small grain population in a debris disk. Because gravitational stirring by small objects is inefficient, a disk composed of 1 km objects, can *never* reach the 100 m s^{-1} limit in 1 Gyr or less. Disks composed of 100 km or larger objects can reach the 100 m s^{-1} limit in less than 100 Myr, but these objects cannot be shattered. Kenyon & Bromley (2001) proposed that the shattering limit might be reached more easily in a disk containing a size distribution of planetesimals. They assumed an initial size distribution similar to the results derived from the complete coagulation models of Kenyon & Luu (1999a, b), $N_C \propto r_i^{-q_f}$ with $q_f = 3$. They then varied the maximum mass of this distribution to derive limits on the stirring as a function of mass.

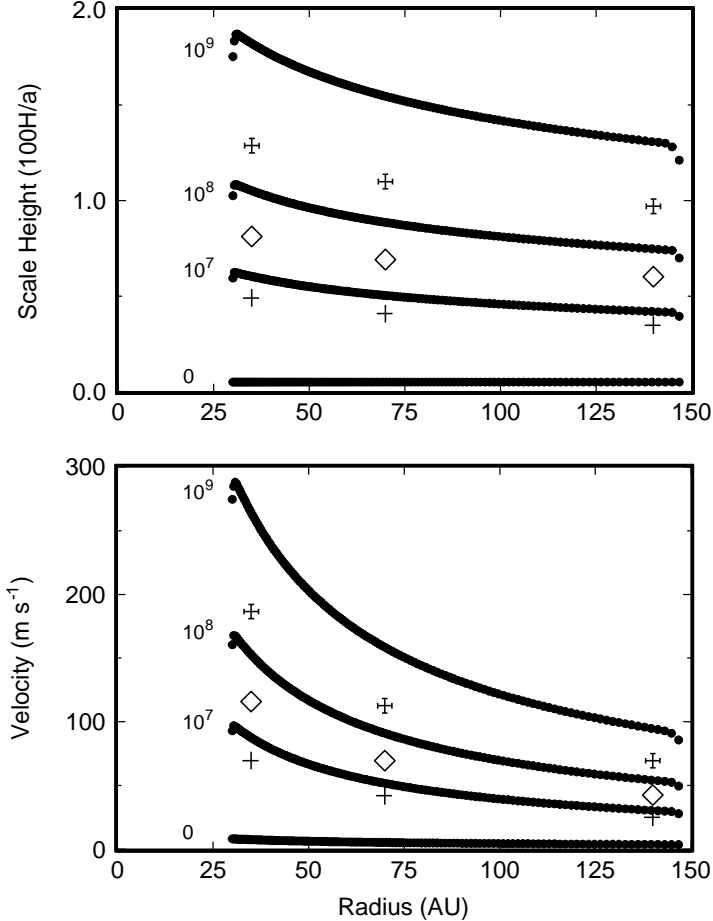


Figure 5 - Evolution of particle velocity (left panel) and vertical scale height (right panel) for 1 m to 1 km planetesimals of a size distribution of 1 m to 500 km planetesimals in a disk surrounding a $3 M_{\odot}$ star. The initial surface density in the disk is $\Sigma = 60 (a/1 \text{ AU})^{-3/2}$. The evolution time in years is listed to the left of each curve. The symbols indicate results for partial disk calculations composed of 16 annuli, instead of the 128 annuli used in the full disk calculation.

Figure 5 shows the evolution of particle velocity (lower panel) and vertical scale height (top panel) for small planetesimals of a size distribution of 1 m to 500 km planetesimals in a disk surrounding a $3 M_{\odot}$ star. The initial surface density in the disk is $\Sigma = 60 (a/1 \text{ AU})^{-3/2}$, somewhat larger than the surface density of a Minimum Mass Solar Nebula. The evolution time in years is listed to the left of each curve. The filled circles show the evolution for a complete disk; the symbols indicate the slower evolution for isolated annuli. Distant gravitational perturbations between large bodies are an important source of velocity evolution (see also Weidenschilling 1989; Stewart & Ida 2000); the evolution of the particle velocity in isolated annuli thus lags results for a complete disk model. These results demonstrate that a few 500 km bodies can stir the velocities of 1 m to 1

km bodies in a circumstellar disk to the shattering limit of 100 m s^{-1} or larger on timescales of 10^7 or more years. The scale height H_d of the dust reaches the observable limit of $100 H_d/A = 1$, on a similar timescale. In contrast, stirring by 100 km bodies is ineffective on 1 Gyr timescales (see Figure 6 of Kenyon & Bromley 2001). Thus, if large bodies embedded in a planetesimal disk are responsible for the large observed velocities of small bodies, these calculations show that the large bodies must have radii of 500 km or larger.

Although these calculations are too new for detailed comparisons with observations, observed scale height profiles of debris disk systems will eventually place useful constraints on the models. The scale height distribution of $H \propto r^{3/4}$ in Figure 5 is shallower than the typical distribution observed in β Pic and other systems $H \propto r$ (e.g., Artymowicz 1997; Lagrange *et al.* 2000). Radiation pressure on shattered grains in the inner portions of the disk should increase the scale height at larger radii; Poynting-Robertson drag on shattered grains in the outer parts of the disk should decrease the scale height at small radii. Coagulation tends to produce larger objects in the inner portions of the disk and should produce larger scale heights in the inner disk. Future calculations will allow us to see how these competing physical processes act on the observed scale height. However, we are encouraged that the scale height distribution derived solely from the stirring calculations is close to those observed in real debris disk systems.

3.4. Summary

The particle-in-a-box formulation works well during the early stages of planet formation. When the number of small planetesimals is large, the distribution of bodies is well-approximated by a uniform density in a narrow grid; the collision rates and velocity evolution can then be treated using fairly simple statistical formulae. More general n -body calculations confirm the basic features of particle-in-a-box calculations for the early stages of planet growth described here (Ida & Makino 1992; Kokubo & Ida 1996). The method begins to break down in the late stages of planetary growth, when the number of large planets is small and one-on-one interactions are important. Direct n -body calculations are then more accurate, but these models cannot follow the numerous small bodies left over from the growth of a few very large objects (e.g., Chambers & Wetherill 1998; Nagasawa *et al.* 2000). Because small objects can contain a substantial fraction of the initial disk mass, they make important contributions to the dynamical evolution of the largest objects throughout the evolution. Several groups are now trying to merge coagulation calculations with direct n -body codes (see, for example, Weidenschilling *et al.* 1997). These hybrid codes should allow better calculations of planet formation from “start to finish.”

4. Tests of Coagulation Models

Most coagulation codes have numerous free parameters which are poorly constrained by theory. For example, algorithms to compute the debris produced in a collision between two or more bodies require as input the tensile strength, S_0 ; the gravitational binding energy, S_g ; the velocity of the ejecta as a function of mass, $f(> v)$; and the number distribution of the ejecta, $n(M)$. Some of

these parameters can be constrained by laboratory experiments on Earth, but some cannot. Until very recently, our solar system has been the only external laboratory to test models. Aside from obvious tests of calculations to attain the masses of the planets in our solar system, comparisons between calculations and solar system data yield constraints on the bulk properties of asteroids and other rocky objects in the inner solar system (e.g., Davis *et al.* 1985, 1994) and on physical processes such as gas drag and Poynting-Robertson drag (see, for example, Burns *et al.* 1979, Kary *et al.* 1993, and references therein). Here we describe several tests of the coagulation code based on objects in the outer solar system.

Kenyon & Luu (1999b) showed that complete coagulation calculations for the outer solar system yield a power law number distribution,

$$\log N_C = N_0 \left(\frac{m}{m_0} \right)^{-a}, \quad (10)$$

where N_C is the cumulative number of bodies with mass larger than m . Both m_0 and N_0 are scaling parameters which depend on the initial mass in the disk. The power law exponent, a , has a small range for the largest bodies – $a = 4.00 \pm 0.25$ – which is fairly independent of the initial conditions and uncertain physical parameters for fragmentation and other processes. This result leads to a direct prediction for the observed luminosity function (LF) of bodies in the Kuiper Belt beyond the orbit of Neptune:

$$\log N = \alpha(R - R_0), \quad (11)$$

where N is the cumulative number of objects brighter than magnitude R and R_0 is a reference magnitude. Coagulation models with $a = 4$ predict $\alpha = 0.6$; observations yield $\alpha = 0.5\text{--}0.7$.

Figure 6 compares model luminosity functions of KBOs with observations. Data are as indicated in the legend of each panel. The open circle with the central dot is the position of Pluto for an adopted albedo of 4%; other observations are from the literature (see Kenyon & Luu 1999b). Error bars for each datum – typically a factor of 2–3 – are not shown for clarity. The lines plot luminosity functions for models with (a) left panel: an initial eccentricity $e_0 = 10^{-3}$ for planetesimals with radii of 1–100 m and $M_0 \approx 0.3$ (dot-dashed), 1.0 (solid), and 3.0 (dashed) times the Minimum Mass Solar Nebula and (b) right panel: a Minimum Mass Solar Nebula with $e_0 = 10^{-2}$ (dashed), $e_0 = 10^{-3}$ (solid), and $e_0 = 10^{-4}$ (dot-dashed). The pair of vertical solid lines indicates the planned magnitude range accessible to *NGST*. The model luminosity functions agree well with current observations.

The good agreement between models and observations for $R = 20\text{--}26$ in Figure 6 is encouraging. The major uncertainties in this comparison – the orbit distribution of KBOs and the evolution of the luminosity function with time – are difficult to quantify. As ground-based telescopes reveal more KBOs, the improved distribution of KBO orbits will yield a more reliable comparison with the models. Collisional erosion over the age of the solar system probably does not affect large KBOs (Davis & Farinella 1997), but dynamical encounters with Neptune can remove large KBOs from the population. This process cannot change

the slope of the luminosity function, but it can change the scaling parameter by a factor of 2 or more (Holman & Wisdom 1993).

Other tests of KBO coagulation models can be made with other data. In our models, disruption of colliding planetesimals can prevent the growth of large objects if the intrinsic tensile strength of the bodies is small (Kenyon & Luu 1999a). If Pluto formed by coagulation, the minimum tensile strength for Kuiper Belt objects in the outer solar system is $S_0 = 300$ erg g⁻¹ (see Ryan *et al.* 1999 for laboratory experiments appropriate for collisions among Kuiper Belt objects). The debris produced by colliding planetesimals should follow a size distribution with $q_f \approx 3.5$, somewhat shallower than the slope of the merger population, $q_f \approx -4$ (Dohnanyi 1969; Davis & Farinella 1997). Our models predict that this transition should occur for objects with radii of ~ 1 km (Kenyon & Luu 1999a). Kenyon & Windhorst (2000) used Olbers Paradox and the measured brightness of the optical night sky to show that the faint end of the size distribution for Kuiper Belt objects has $q_f \lesssim -3.5$ for objects with sizes of 1 m to 1 km. Observations with *NGST* can search for a break in the slope of the size distribution at 1 km ($R \approx 30$), as illustrated in Figure 6.

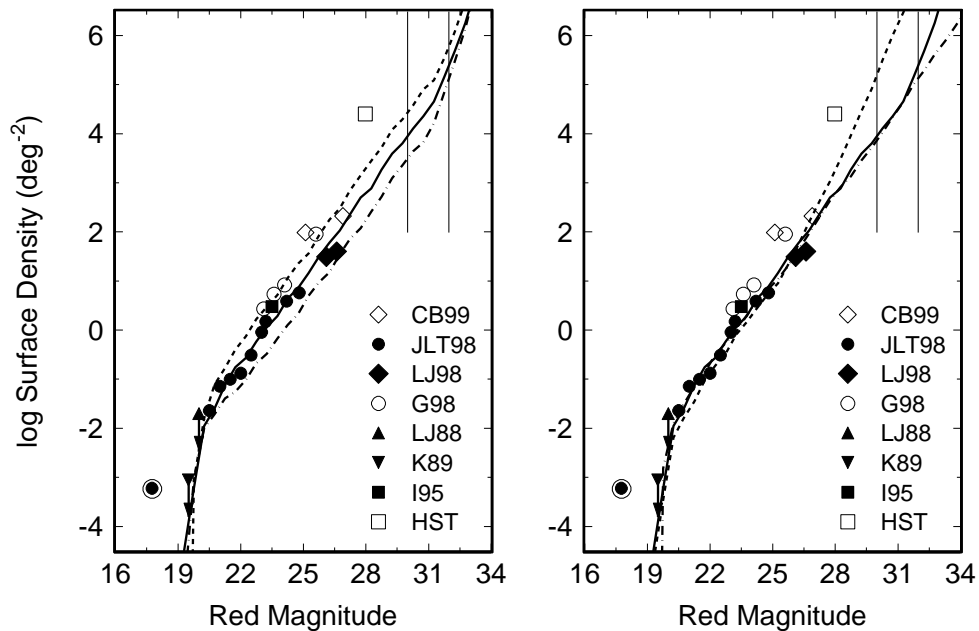


Figure 6 - Comparison of model luminosity functions of KBOs with observations. Data are as indicated in the legend of each panel. The open circle with the central dot is the position of Pluto for an adopted albedo of 4%; other observations are from Cochran *et al.* (1998; HST), Irwin *et al.* (1995; I95), Kowal 1989 (1989; K89), Luu & Jewitt (1988; LJ88), Gladman *et al.* (1998; G98), Luu & Jewitt (1998; LJ98), Jewitt *et al.* (1998; JLT98) and Chiang & Brown (1999; CB99). Error bars for each datum – typically a factor of 2–3 – and the upper limit from Levison & Duncan (1990) are not shown for clarity. The lines plot luminosity functions for models with (a) left panel: $e_0 = 10^{-3}$ and $M_0 \approx 0.3$ (dot-dashed), 1.0 (solid), and 3.0 (dashed) times the Minimum Mass Solar Nebula and (b) right panel: a Minimum Mass Solar Nebula with $e_0 = 10^{-2}$ (dashed), $e_0 = 10^{-3}$ (solid), and $e_0 = 10^{-4}$ (dot-dashed). A Minimum Mass Solar Nebula has $M_0 \approx 12 M_\oplus$ within $R = 42$ –50 AU. The pair of vertical solid lines indicates the planned magnitude range accessible to *NGST*.

Observations of debris disk systems provide other measurements of the slope of the size distribution for small objects. The data are consistent with the predicted slopes, but the uncertainties remain large (see Kenyon *et al.* 1999; Lagrange *et al.* 2000).

In addition to the geometry and mass estimates derived from images and spectral energy distributions, many observations of debris disk systems have concentrated on measurements of the composition and other bulk properties of solid objects (see Pantin *et al.* 1997, Lagrange *et al.* 2000, and references therein). Many systems show evidence for infalling ‘comets’ and other gaseous phenomena in the disk (e.g., Beust *et al.* 1998, Grady *et al.* 1999, Sitko *et al.* 1999, Lagrange *et al.* 2000, and references therein). Although coagulation calculations do not address directly questions concerning the composition of solid bodies in debris disks, calculations will eventually yield accurate rates of dust infall and ejection for comparison with observations.

5. Summary

Understanding whether or not coagulation or dynamical instability produce solar systems similar to those we observe involves a comparison of detailed numerical calculations with high quality observations. The advent of fast, parallel computers now allows fairly realistic calculations of the complete evolution of part of a solar system; calculations of an entire solar system will be possible in 10 years or less. Observations with ground-based and space-based telescopes now provide data with sufficient sensitivity and spatial resolution to make direct tests of some predictions of the detailed numerical calculations. These tests yield a better understanding of the physical processes involved in forming terrestrial planets like the Earth and gas giant planets like Jupiter. As both the data and models improve, we will have a better grasp of the origin of planetary systems similar to our own.

In addition to the tests described in §4, ground-based and space-based observations will yield new tests of planet formation theories. Data from *SIRTF*, *SOFIA*, and other NASA-sponsored missions will result in many new debris disk systems and better estimates for the distribution of lifetimes for these systems. Comparisons with the results of the coagulation calculations will test theories of the collisional cascade. Direct detection of more large Kuiper Belt objects will test predictions for the merger population; direct detection of the optical and far-infrared background from KBOs will test predictions for the size distribution of the debris population and a measurement of the albedo of KBOs (Kenyon & Windhorst 2000). These comparisons – combined with new calculations for the Kuiper Belt as in Kenyon & Luu (1998, 1999) – will give us a better understanding of planet formation (for Earth-sized planets) in the outer part of a solar system.

Along with simple observational comparisons of the disk lifetime, inclusion of good models for gas drag, Poynting-Robertson drag, and radiation pressure on grains will allow predictions for the surface brightness profile of solar system disks, derived from the model results in Figure 5. The *HST* and several ground-based telescopes have derived observed surface brightness profiles; the *NGST* mission will provide many hundreds. Comparisons of observations with

coagulation model predictions will allow better constraints on the models and on the physical situation in extra-solar debris disks. The identification of features in the observed profiles may yield constraints on planetary masses in the disks.

Observations may also help guide theorists in producing better models for gas giant planets. Current theory has trouble understanding the formation of gas giants at distance of $\gtrsim 10$ AU (coagulation models) and $\gtrsim 20$ AU (dynamical instability models) from the central star. Identification of gas giant planets in other solar systems at large distances from their parent star would provide a stern test of either model. Discovery of gas giants in the weak-emission T Tauri stars (wTTs) might be the sternest test of all. Many wTTs have little or no evidence for emission from disk material at $A \lesssim 1-10$ AU, suggesting that planet formation may be complete in these systems. A gas giant planet discovered beyond 20 AU from the central star in a wTTS would probably be luminous due to its young age and might yield important insights into the formation of gas giant planets.

I would like to thank Jane Luu. Without Jane's foresight and persistence, our joint projects on planet formation would never have been possible. I also thank B. Bromley, A. Cameron, F. Franklin, M. Geller, M. Holman, and J. Wood for advice and comments. I also acknowledge generous allotments of computer time on the JPL Cray T3D 'Cosmos', the HP Exemplar 'Neptune' and the Silicon Graphics Origin-2000 'Alhena' through funding from the NASA Offices of Mission to Planet Earth, Aeronautics, and Space Science.

References

- Adachi, I., Hayashi, C., Nakazawa, K. 1976, *Progress of Theoretical Physics* 56, 1756
- Artymowicz, P. 1997, *ARE&PS*, 25, 175
- Artymowicz, P., Burrows, C., & Paresce, F. 1989, *ApJ*, 337, 494
- Augereau, J. C., Lagrange, A.-M., Mouillet, D., Papaloizou, J. C. B., & Grorod, P. A. 1999, *A&A*, 348, 557
- Aumann, H. H. *et al.* , 1984, *ApJ*, 278, L23
- Backman, D. E., Dasgupta, A., & Stencel, R. E. 1995, *ApJ*, 450, L35
- Backman, D. E., & Paresce, F. 1993, in *Protostars and Planets III*, eds. E. H. Levy & J. I. Lunine, Tucson, Univ of Arizona, p. 1253
- Bailey, M. 1994, In *Asteroids, Comets, Meteors 1993*, edited by A. Milani, M. DiMartino, and A. Cellino, Kluwer Academic Publishers, Dordrecht, p. 443
- Balbus, S. A., & Hawley, J. F. 1998, *Rev Mod Phys*, 70, 1
- Balbus, S. A., Hawley, J. F., & Stone, J. M. 1996, *ApJ*, 467, 76
- Bally, J., Sutherland, R. S., Devine, D., & Johnstone, D. 1998, *AJ*, 116, 293
- Barge, P., and Pellat, R. 1990, *Icarus*, 85, 481

- Beckwith, S. V. W. 1999, in *The Physics of Star Formation and Early Stellar Evolution*, edited by C. J. Lada and N. Kylafis, Dordrecht, Kluwer, p. 579
- Bell, K. R., & Lin, D. N. C. 1994, ApJ, 427, 987
- Bell, K. R., Lin, D. N. C., Hartmann, L., & Kenyon, S. J. 1995, ApJ, 444, 376
- Beust, H., Lagrange, A.-M., Crawford, I. A., Goudard, C., Spyromilio, J., Vidal-Madjar, A. 1998, A&A, 338, 1015
- Bodenheimer, P., Hubickyj, O., & Lissauer, J. 2000, Icarus, 143, 2
- Boss, A. P. 1997, Science, 276, 1836
- Boss, A. P. 2000, ApJ, 536, 101
- Burns, J. A., Lamy, P. L., & Soter, S. 1979, Icarus, 40, 1
- Cameron, A. G. W. 1995, Meteoritics, 30, 133
- Chambers, J. E., & Wetherill, G. W. 1998, Icarus, 136, 304
- Chiang, E. I., & Brown, M. E. 1999, AJ, 118, 1411
- Chiang, E. I., & Goldreich, M. E. 1997, ApJ, 490, 368
- Chiang, E. I., & Goldreich, M. E. 1999, ApJ, 519, 279
- Cochran, A. L., Levison, H. F., Tamblyn, P., Stern, S. A., & Duncan, M. 1998, ApJ, 455, L89
- Cuzzi, J. N., Dobrovolskis, A. R., & Champney, J. M. 1993, Icarus, 106, 102
- Cochran, W. D., Hatzes, A. P., Butler, P. R., & Marcy, G. W. 1997, ApJ, 483, 457
- Davis, D. R., Chapman, C. R., Weidenschilling, S. J., & Greenberg, R. 1985, Icarus, 62, 30
- Davis, D. R., & Farinella, P. 1997, Icarus, 125, 50
- Davis, D. R., Ryan, E. V., & Farinella, P. 1994, Planet. Space Sci., 42, 599
- DelFosse, X., *et al.* 1998, A&A, 338, L67
- Dohnanyi, J. W. 1969, J. Geophys. Res., 74, 2531
- Duncan, M. J., Levison, H. F., & Budd, S. M. 1995, AJ, 110, 3073
- Duncan, M., Quinn, T., & Tremaine, S. 1987, AJ, 94, 1330
- Fernández, J. A. 1997, Icarus, 129, 106
- Fernández, J. A., & Ip, W.-H. 1984, Icarus, 58, 109
- Ford, E. B., Rasio, F. A., & Sills, A. 1999, ApJ, 514, 411
- Gladman, B., Kavelaars, J. J., Nicholson, P. D., Loredo, T. J., & Burns, J. A. 1998, AJ, 116, 2042
- Goldreich, P., & Ward, W. R. 1973, ApJ, 183, 1051
- Grady, C. A., Pérez, M. R., Bjorkman, K. S., & Massa, D. 1999, ApJ, 511, 925
- Greaves, J. S. *et al.* 1998, ApJ, 506, L133
- Greenberg, R., Wacker, J. F., Hartmann, W. K., & Chapman, C. R. 1978, Icarus, 35, 1
- Greenberg, R., Weidenschilling, S. J., Chapman, C. R., Davis, D. R. 1984, Icarus, 59, 87

- Harris, A. W. 1978, in *The Origin of the Solar System*, edited by S. F. Dermott, p. 469
- Hartmann, L. 1998, *Accretion Processes in Star Formation*, Cambridge, Cambridge University Press
- Hartmann, L., Calvet, N., Gullbring, E., & D'Alessio, P. 1998, ApJ, 495, 385
- Hartmann, L., & Kenyon, S.J. 1985, ApJ, 299, 462
- Hartmann, L., & Kenyon, S. J. 1996, ARA&A, 34, 207
- Hartmann, L., & Raymond, L. 1984, ApJ, 276, 560
- Hayashi, C. 1981, Prog Theor Phys Suppl, 70, 35
- Hayashi, C., Nakazawa, K., & Nakagawa, Y. 1985, In *Protostars and Planets II*, eds. 4 (U. of Arizona Press, Tucson, pp. 1100 - 1153
- Hollenbach, D. J., Yorke, H. W., & Johnstone, D. 2000, in *Protostars & Planets IV*, edited by V. Mannings, A. P. Boss, & S. S. Russell, Tucson, Univ. of Arizona, p. 401
- Hollenbach, D. J., Johnstone, D., Lizano, S., & Shu, F. 1994, ApJ, 428, 654
- Holman, M. J., & Wisdom, J. 1993, AJ, 105, 1987
- Hornung, P., Pellat, R., & Barge, P. 1985 Icarus, 64, 2951
- Hoyle, F. 1946, MNRAS, 106, 406
- Ida, S., Larwood, J., & Burkert, A. 2000, ApJ, 528, 351
- Ida, S., & Makino, J. 1992, Icarus, 96, 107
- Ida, S., & Makino, J. 1993, Icarus, 106, 210
- Ip, W.-H. 1989, Icarus, 80, 167
- Irwin, M., Tremaine, S., & Źytkow, A. N. 1995, AJ, 10, 3082
- Jayawardhana, R. *et al.* 1998, ApJ, 503, L79
- Jayawardhana, R. *et al.* 1999, ApJ, 521, L129
- Jewitt, D., & Luu, J. 1993, Nature, 362, 730
- Jewitt, D., Luu, J., & Chen, J. 1996, AJ, 112, 1225
- Jewitt, D., Luu, J. X., & Trujillo, C. 1998, AJ, 115, 2125
- Johnstone, D., Hollenbach, D., & Bally, J. 1998 ApJ, 499, 758
- Kalas, P., & Jewitt, D. 1995, AJ, 110, 794
- Kalas, P., Larwood, J., Smith, B. A., & Schultz, A. 2000, ApJ, 530, L133
- Kary, D. M., Lissauer, J. J., & Greenzweig, Y. 1993, Icarus, 106, 268
- Kenyon, S. J. 1999, in *The Physics of Star Formation and Early Stellar Evolution*, edited by C. J. Lada and N. Kylafis, Dordrecht, Kluwer, p. 613
- Kenyon, S. J., & Bromley, B. C. 2001, AJ, 121, No. 1 (astro-ph/0009185)
- Kenyon, S. J., & Hartmann, L. 1987, ApJ, 323, 714
- Kenyon, S. J., & Luu, J. X. 1998, AJ, 115, 2136
- Kenyon, S. J., & Luu, J. X. 1999a, AJ, 118, 1101
- Kenyon, S. J., & Luu, J. X. 1999b, ApJ, 526, 465
- Kenyon, S. J., & Windhorst, R. A. 2001, ApJ, submitted (astro-ph/0009162)
- Kenyon, S. J., Wood, K., Whitney, B. A., & Wolff, M. 1999, ApJ, 524, L119
- Klahr, H. H., & Lin, D. N. C. 2000, AJ, in press (astro-ph/0007422)

- Kley, W. 2000, MNRAS, 313, L47
- Koerner, D. W., Ressler, M. E., Werner, M. W., & Backman, D. E. 1998, ApJ, 503, L83
- Kokubo, E., & Ida, S. 1996, Icarus, 131, 171
- Kortenkamp, S. J., & Wetherill, G. W. 2000, Icarus, 143, 60
- Kowal, C. T. 1989, Icarus, 77, 118
- Lada, C. J. 1999, in *The Physics of Star Formation and Early Stellar Evolution*, edited by C. J. Lada and N. Kylafis, Dordrecht, Kluwer, p. 143
- Lagrange, A.-M., Backman, D., & Artymowicz, P. 2000, in *Protostars & Planets IV*, edited by V. Mannings, A. P. Boss, & S. S. Russell, Tucson, Univ. of Arizona, p. 639
- Larwood, J. D. 1997, MNRAS, 290, 490
- Latham, D. W., Stefanik, R. P., Mazeh, T., Mayor, M., & Murki, G. 1989, ApJ, 339, 38
- Lee, M. H. 2000, Icarus, 143, 74
- Levison, H. F., & Duncan, M. J. 1990, AJ, 100, 1669
- Levison, H. F., Lissauer, J. J., & Duncan, M. J. 1998, AJ, 116, 1998
- Lin, D. N. C., & Ida, S. 1997, ApJ, 477, 781
- Lin, D. N. C., & Papaloizou, J. C. B., 1995, ARA&A, 33, 505
- Lin, D. N. C., & Papaloizou, J. C. B., 1996, ARA&A, 34, 703
- Lissauer, J. J. 1987, Icarus, 69, 249
- Lissauer, J. J. 1993, ARA&A, 31, 129
- Lissauer, J. J. 1995, Icarus, 114, 217
- Lissauer, J. J., Pollack, J. B., Wetherill, G. W., & Stevenson, D. J. 1996, in *Neptune and Triton*, edited by D. P. Cruikshank, M. S. Matthews, & A. M. Schumann, U. of Arizona Press, Tucson, 37
- Luciani, J. F., Namouni, F., & Pellat, R. 1995, ApJ, 439, 800
- Lüst, R. 1952, Zs. f. Nat., 7a, 87
- Luu, J. X., & Jewitt, D. 1988, AJ, 85, 1256
- Luu, J. X., & Jewitt, D. 1998, ApJ, 502, L91
- Luu, J. X., Marsden, B., Jewitt, D., Trujillo, C. A., Hergenother, C. W., Chen, J., & Offutt, W. B. 1997, Nature, 387, 573
- Malhotra, R. 1995, AJ, 110, 420
- Malyshkin, L., & Goodman, J. 2000, astro-ph/0004070
- Marcy, G. W., & Butler, R. P. 1999, in *The Physics of Star Formation and Early Stellar Evolution*, edited by C. J. Lada and N. Kylafis, Dordrecht, Kluwer, p. 681
- Marcy, G. W., & Butler, P. R. 1996, ApJ, 464, L133
- Morbidelli, A., & Valsecchi, G. B. 1997, Icarus, 128, 464
- Nagasawa, M., Tanaka, H., & Ida, S. 2000, AJ, 119, 1480
- Nakagawa, Y., Hayashi, C., & Nakazawa, K. 1983, Icarus, 54, 361
- Najita, J. R., & Shu, F. H. 1994, ApJ, 429, 808

- Noyes, R. W. *et al.* 1997, *ApJ*, 483, L111
- Ostriker, E. C., & Shu, F. H. 1995, *ApJ*, 447, 813
- Pantin, E., Lagage, P. O., & Artymowicz, P. 1997, *A&A*, 327, 1123
- Podolak, M., & Reynolds, R. T. 1987, *Icarus*, 70, 31
- Podolak, M., Young, R., & Reynolds, R. 1985, *Icarus*, 63, 266
- Pollack, J. B. 1984, *ARA&A*, 22, 389
- Pollack, J. B., Hubickyj, O., Bodenheimer, P., Lissauer, J. J., Podolak, M., & Greenzweig, Y. 1996, *Icarus*, 124, 62
- Proga, D. 2000, *ApJ*, 538, 684
- Proga, D., Stone, J. M., & Drew, J. E. 1998, *MNRAS*, 295, 595
- Richling, S., & Yorke, H. W. 1997, *A&A*, 327, 317
- Richling, S., & Yorke, H. W. 1998, *A&A*, 340, 508
- Richling, S., & Yorke, H. W. 2000, *ApJ*, 539, 258
- Ruden, S. P., & Pollack, J. B. 1991, *ApJ*, 375, 740
- Russell, S. S., Srinivasan, G., Huss, G. R., Wasserburg, G. J., & Macpherson, G. J. 1996, *Science*, 273, 757
- Ryan, E. V., Davis, D. R., Giblin, I. 1999, *Icarus*, 142, 56
- Safronov, V. S. 1969, Evolution of the Protoplanetary Cloud and Formation of the Earth and Planets, Nauka, Moscow [Translation 1972, NASA TT F-677]
- Sasselov, D. D., & Lecar, M. 2000, *ApJ*, 528, 995
- Schneider, G., *et al.* 1999, *ApJ*, 513, L127
- Sekiya, M., & Ishitsu, N. 2000, *Earth Planets Space*, 52, 517
- Shu, F. H., Johnstone, D., & Hollenbach, D. 1993, *Icarus*, 106, 92
- Shu, F. H., Najita, J., Ostriker, E., Wilkin, F., Ruden, S. P., & Lizano, S. 1994a, *ApJ*, 429, 781
- Shu, F. H., Najita, J., Ruden, S. P., & Lizano, S. 1994b, *ApJ*, 429, 797
- Sitko, M. L., Grady, C. A., Lynch, D. K., Russell, R. W., & Hanner, M. S. 1999, *ApJ*, 510, 408
- Smith, B. A., & Terrile, R. J. 1984, *Science*, 226, 1421
- Spaute, D., Weidenschilling, S. J., Davis, D. R., & Marzari, F. 1991, *Icarus*, 92, 147
- Stern, S. A. 1995, *AJ*, 110, 856
- Stern, S. A. 1996, *AJ*, 112, 1203
- Stern, S. A., & Colwell, J. E. 1997a, *AJ*, 114, 841
- Stern, S. A., & Colwell, J. E. 1997b, *ApJ*, 490, 879
- Stone, J. M., Gammie, C. F., Balbus, S. A., & Hawley, J. F. 2000, in *Protostars and Planets IV*, edited by V. Mannings, A. P. Boss, & S. S. Russell, Tucson, Univ. of Arizona Press, p. 589
- von Weizsäcker, C. F. 1943, *Zs. f. Ap.*, 22, 319
- von Weizsäcker, C. F. 1948, *Zs. f. Nat.*, 3a, 524
- Weidenschilling, S. J. 1977, *Ap Sp Sci*, 51, 153

- Weidenschilling, S. J. 1980, Icarus, 44, 172
- Weidenschilling, S. J. 1989, Icarus, 80, 179
- Weidenschilling, S. J., & Cuzzi, J. N., 1993, in *Protostars and Planets III*, edited by E. H. Levy & J. I. Lunine, Tucson, Univ of Arizona, p. 1031
- Weidenschilling, S. J., & Marzari, F. 1996, Nature, 384, 619
- Weidenschilling, S. J., Spaute, D., Davis, D. R., Marzari, F., Ohtsuki, K. 1997, Icarus, 128, 429
- Wetherill, G. W., & Stewart, G. R. 1989, Icarus, 77, 300
- Wetherill, G. W., & Stewart, G. R. 1993, Icarus, 106, 190
- Williams, I. P., O'Ceallaigh, D. P., Fitzsimmons, A., Marsden, B. G. 1995, Icarus, 116, 180
- Wurm, G., & Blum, J. 1998, Icarus, 132, 125
- Wurm, G., & Blum, J. 2000, ApJ, 529, L57, 125